INTERNATIONAL JOURNAL FOR NUMERICAL METHODS IN FLUIDS
*Int. J. Numer. Meth. Fluids* (2009)
Published online in Wiley InterScience (www.interscience.wiley.com). DOI: 10.1002/fld.2046

# Consistent discretization for simulations of flows with moving generalized curvilinear coordinates

Y. J. Chou*, † and O. B. Fringer

*Environmental Fluid Mechanics Laboratory, Stanford University, Stanford, CA 94305-4020, U.S.A.*

SUMMARY

We develop a consistent discretization of conservative momentum and scalar transport for the numerical simulation of flow using a generalized moving curvilinear coordinate system. The formulation guarantees consistency between the discrete transport equation and the discrete mass conservation equation due to grid motion. This enables simulation of conservative transport using generalized curvilinear grids that move arbitrarily in three dimensions while maintaining the desired properties of the discrete transport equation on a stationary grid, such as constancy, conservation, and monotonicity. In addition to guaranteeing consistency for momentum and scalar transport, the formulation ensures geometric conservation and maintains the desired high-order time accuracy of the discretization on a moving grid. Through numerical examples we show that, when the computation is carried out on a moving grid, consistency between the discretized scalar advection equation and the discretized equation for flow mass conservation due to grid motion is required in order to obtain stable and accurate results. We also demonstrate that significant errors can result when non-consistent discretizations are employed. Copyright © 2009 John Wiley & Sons, Ltd.

Received 28 August 2008; Revised 10 February 2009; Accepted 12 February 2009

KEY WORDS: finite-volume method; scalar transport; incompressible flow; CWC; curvilinear coordinate

## 1. INTRODUCTION

A number of problems in computational fluid dynamics (CFD) require flow calculations on moving-grid systems. Grid movement usually is employed for simulations that employ adaptivity designed to resolve strong gradients in the flow as the solution progresses or simulations involving moving boundaries. Typical examples of the former case include simulations of shock waves or the transport

*Correspondence to: Y. J. Chou, Department of Civil and Environmental Engineering, Stanford University, Stanford, CA 94305-4020, U.S.A.
†E-mail: yjchou@stanford.edu

Contract/grant sponsor: Publishing Arts Research Council; contract/grant number: 98-1846389
Contract/grant sponsor: ONR Coastal Geosciences Program; contract/grant number: N00014-05-1-0177

Copyright © 2009 John Wiley & Sons, Ltd.

of sharp scalar fronts, while examples of the latter case can be found in flutter simulation of wings, turbomachinery, or some geophysical flow applications (e.g. free-surface flows and flows over dynamic bed forms). Typically, when flow problems are solved on dynamic meshes, grid motion cannot be based solely on a naive flow-following algorithm [1], since severe grid deformation can result particularly in flows with high strain rates. Therefore, in a generalized moving-grid flow simulation, grid position must be exactly prescribed such that grid quality is guaranteed at each time step. In problems that involve boundary movement, desired grid quality is automatically satisfied by the grid generation function at each time step. For problems in which grids move based on the solution itself, grid motion is specified through monitor functions which guarantee grid quality while resolving as much of the fine flow features as possible.

While grid quality is important for accurate flow simulations, it is also important to maintain consistency between discrete fluid mass transport due to grid motion and the discrete transport equations for momentum and scalars. This implies that the same method that is used to compute the divergence of the flux of momentum and the scalars must be used to compute the divergence of fluid mass in a moving grid if one desires to maintain the properties of the fixed-grid discretization. This consistency condition is known as consistency with continuity (CWC) and is an essential requirement for conservation on fixed grids and has been discussed by various authors [2–5] in the context of higher-order conservative transport schemes. For non-moving grids, CWC implies that the discrete divergence operater that is used for the continuity equation must be identical to the discrete divergence operater that is used for the divergence of the flux of some scalar. It is straightforward to ensure CWC with non-moving Cartesian grids, but special care must be taken when developing CWC schemes on moving grids. For example, Gross *et al.* [6] studied the CWC condition for the simulation of free-surface flow on Cartesian grids and observed large errors and strongly non-monotonic behavior when CWC is violated, despite the use of monotonic transport schemes designed for fixed grids. They showed how consistent discretizations can be employed if special care is taken when discretizing the scalar transport equation.

According to Lin and Rood [3], a convenient definition of CWC is, *a discretization of the advection equation is consistent with continuity if, given a spatially uniform scalar field as an initial datum, and a general flow field, the discretized scalar advection equation reduces to the discretized continuity equation*, which applies whether or not the grid geometry varies in time. This statement is similar to that described for the discrete geometric conservation law (DGCL) in the arbitrary Lagrangian–Eulerian scheme, which states that the discretized equation on moving meshes must be able to preserve a constant solution such that while substituting a constant solution field into the transport equation, the discrete version of the geometric conservation law (GCL) is recovered. The GCL was first addressed by Thomas and Lombard [7] in 1978, in which a first-order accurate in time method was presented for solving flow problems on dynamic meshes while preserving grid geometry. More recently, derivations have shown that the DGCL is a sufficient condition for achieving first-order time accuracy [8] but not a sufficient condition for obtaining the design accuracy of the underlying time-integration scheme when it is greater than one [9]. It has been demonstrated that the DGCL is a sufficient and necessary condition for preserving the nonlinear stability of the underlying time-integration scheme for the finite-volume formulation [10], but not necessarily for the finite element formulation [11, 12]. As demonstrated in the present paper, failure to satisfy CWC would result in the violation of the DGCL, thus the stability properties derived in References [10–12] for the DGCL also apply to CWC in the present context.

In this study we develop a method to discretize the equations of motion and transport that is consistent with the discrete continuity equation on a moving generalized curvilinear coordinate grid.

Copyright © 2009 John Wiley & Sons, Ltd.

DOI: 10.1002/fld

It is demonstrated that violation of CWC is equivalent to the violation of DGCL, thereby introducing excessive mass. We develop a technique to calculate the grid velocities that satisfies the CWC condition and maintains the second-order accuracy of the original fixed-grid code in three-dimensional space. To this end, a moving-grid algorithm along with the CWC discretization procedure is applied to a three-dimensional Navier–Stokes code to allow for the simulation of incompressible flow on a generalized moving curvilinear coordinate grid. CWC and non-CWC are demonstrated with examples that include pure grid advection in a three-dimensional deforming computational domain and flow induced by an oscillating boundary.

## 2. MATHEMATICAL FORMULATION

### *2.1. Governing equations*

The equation governing the conservation of a certain physical property $\phi$ on a fixed Cartesian grid is given by

$$\frac{\partial \phi}{\partial t} + \frac{\partial}{\partial x_j}(\phi u_j) = \mathscr{S} \tag{1}$$

where the Einstein summation convention is assumed, $j = 1, 2, 3$, $u_j$ is the $j$th component of the Cartesian velocity and $\mathscr{S}$ represents a source or sink. In this paper, hydrodynamic and scalar transport problems are studied, and hence Equation (1) represents conservation of momentum if $\phi = u_i (i = 1, 2, 3)$, mass of fluid if $\phi = \rho =$ fluid density, or scalar mass if $\phi = C =$ scalar concentration. When a moving-grid simulation is carried out in a curvilinear coordinate system, through the transformation between the fixed Cartesian coordinate system $(x_1, x_2, x_3)$ and the moving curvilinear coordinate system $(\xi_1, \xi_2, \xi_3)$ [13], the transformed curvilinear coordinate equations in strong conservation law form [14] reads

$$\frac{\partial}{\partial t}(J^{-1}\phi) + \frac{\partial}{\partial \xi_m}(\phi U_m) - \frac{\partial}{\partial \xi_m}(\phi U_{g,m}) = S \tag{2}$$

Here

$$J^{-1} = \det\left(\frac{\partial x_i}{\partial \xi_j}\right) \tag{3}$$

is the inverse of the Jacobian of transformation and represents the ratio of the volume of a computational cell in physical space to its volume in computational space, the contravariant volume flux is

$$U_m = J^{-1}\frac{\partial \xi_m}{\partial x_j} u_j \tag{4}$$

and the contravariant volume flux associated with the grid velocity $u_{g,j}$ is given by

$$U_{g,m} = J^{-1}\frac{\partial \xi_m}{\partial x_j} u_{g,j} = J^{-1}\frac{\partial \xi_m}{\partial x_j}\frac{\mathrm{d}x_{g,j}}{\mathrm{d}t} \tag{5}$$

Copyright © 2009 John Wiley & Sons, Ltd.

DOI: 10.1002/fld

Therefore, the set of equations representing conservation of fluid mass, momentum, and scalar mass in a generalized moving curvilinear coordinate are given by, respectively,

$$\frac{\partial}{\partial t}(J^{-1}\rho)+\frac{\partial}{\partial \xi_m}(\rho U_m)-\frac{\partial}{\partial \xi_m}(\rho U_{g,m})=0 \tag{6}$$

$$\frac{\partial}{\partial t}(J^{-1}u_i)+\frac{\partial}{\partial \xi_m}(u_i U_m)-\frac{\partial}{\partial \xi_m}(u_i U_{g,m})=S_{u_i} \tag{7}$$

and

$$\frac{\partial}{\partial t}(J^{-1}C)+\frac{\partial}{\partial \xi_m}(C U_m)-\frac{\partial}{\partial \xi_m}(C U_{g,m})=S_c \tag{8}$$

where $S_{u_i}$ comprises the effects of pressure, viscous stresses, and body forces while $S_c$ comprises diffusion and any inflow or outflow of scalar mass. For incompressible flow, Equation (6) reduces to

$$\frac{\partial}{\partial t}(J^{-1})+\frac{\partial U_m}{\partial \xi_m}-\frac{\partial U_{g,m}}{\partial \xi_m}=0 \tag{9}$$

This equation shows that the generalized curvilinear coordinate version of the GCL is given by

$$\frac{\partial}{\partial t}(J^{-1})+\frac{\partial U_{g,m}}{\partial \xi_m}=0 \tag{10}$$

which, if satisfied, implies continuity of fluid in generalized curvilinear coordinates,

$$\frac{\partial U_m}{\partial \xi_m}=0 \tag{11}$$

### 2.2. *Finite-volume discretization*

Employing the finite-volume formulation, the discrete two-dimensional form of the scalar advection Equation (8) on a moving grid is given by

$$\begin{aligned}\frac{\mathrm{d}}{\mathrm{d}t}(J^{-1}|_{i,j}C_{i,j}) = &-\frac{1}{\Delta\xi_{i,j}}(C_{i+1/2,j}U_{i+1/2,j}-C_{i-1/2,j}U_{i-1/2,j})\\ &-\frac{1}{\Delta\eta_{i,j}}(C_{i,j+1/2}V_{i,j+1/2}-C_{i,j-1/2}V_{i,j-1/2})\\ &+\frac{1}{\Delta\xi_{i,j}}(C_{i+1/2,j}U_{g,i+1/2,j}-C_{i-1/2,j}U_{g,i-1/2,j})\\ &+\frac{1}{\Delta\eta_{i,j}}(C_{i,j+1/2}V_{g,i,j+1/2}-C_{i,j-1/2}V_{g,i,j-1/2})+S_{c,i,j}\end{aligned} \tag{12}$$

where subscripts $i$ and $j$ are grid indices in the $\xi$- and $\eta$-directions, respectively, $\Delta\xi$ and $\Delta\eta$ are the distances between the curvilinear coordinate grid lines, and the subscript $\frac{1}{2}$ indicates the face value

Copyright © 2009 John Wiley & Sons, Ltd.

DOI: 10.1002/fld

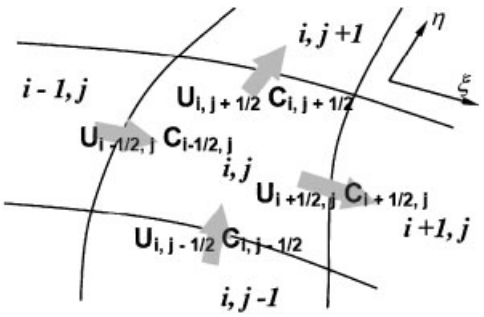


Figure 1. The control volume of a cell $(i, j)$ and the associated face fluxes in the curvilinear coordinate system.

of the cell, as shown in Figure 1. Assuming that $\Delta\xi_{i,j}=\Delta\eta_{i,j}=1$, in the absence of diffusion, sources or sinks, Equation (12) reduces to

$$\begin{aligned}\frac{\mathrm{d}}{\mathrm{d}t}(J^{-1}|_{i,j}C_{i,j}) = &-(C_{i+1/2,j}U_{i+1/2,j}-C_{i-1/2,j}U_{i-1/2,j})\\ &-(C_{i,j+1/2}V_{i,j+1/2}-C_{i,j-1/2}V_{i,j-1/2})\\ &+(C_{i+1/2,j}U_{g,i+1/2,j}-C_{i-1/2,j}U_{g,i-1/2,j})\\ &+(C_{i,j+1/2}V_{g,i,j+1/2}-C_{i,j-1/2}V_{g,i,j-1/2})\end{aligned} \tag{13}$$

For the sake of simplicity, in this paper we discuss the discretized equations in their two-dimensional forms, although addition of the third dimension is straightforward. Equation (13) is a spatially discretized advection equation and can be further discretized in time based on the desired temporal accuracy and stability. For the case of a fixed grid, numerical properties associated with discretization techniques for the scalar advection equation have been extensively studied and the desired numerical properties can be achieved using different discretization techniques as discussed in the literature (see, for example, [5, 15]). However, for the case of a moving grid, as will be discussed in this paper, the accuracy of the numerical discretization of Equation (13) depends highly on the accuracy of the discretized version of the fluid mass conservation Equation (9).

Applying the same finite-volume discretization technique from Equation (13) to the fluid mass conservation Equation (9) gives

$$\begin{aligned}\frac{\mathrm{d}}{\mathrm{d}t}(J^{-1}|_{i,j}) = &(U_{g,i+1/2,j}-U_{g,i-1/2,j})+(V_{g,i,j+1/2}-V_{g,i,j-1/2})\\ &-(U_{i+1/2,j}-U_{i-1/2,j})-(V_{i,j+1/2}-V_{i,j-1/2})\end{aligned} \tag{14}$$

Typical CFD codes for incompressible flow employ some form of a pressure projection method at each time step (e.g. [16–18]) to ensure continuity at the next time step, such that, on a curvilinear grid, at least to the accuracy of the method, local continuity is satisfied, vis.

$$U_{i+1/2,j}-U_{i-1/2,j}+V_{i,j+1/2}-V_{i,j-1/2}=0 \tag{15}$$

Copyright © 2009 John Wiley & Sons, Ltd.

DOI: 10.1002/fld

With local continuity satisfied, volume conservation (14) reduces to the discretized GCL

$$\frac{\mathrm{d}}{\mathrm{d}t}(J^{-1}|_{i,j}) = (U_{g,i+1/2,j} - U_{g,i-1/2,j}) + (V_{g,i,j+1/2} - V_{g,i,j-1/2}) \tag{16}$$

or discrete space conservation law in some contexts (e.g. [19]).

## 3. DISCRETE GEOMETRIC CONSERVATION

### *3.1. GCL with the finite-volume formulation*

Grid motion is typically accomplished by moving the vertices of a finite-volume grid and computing the grid velocities and metrics that change with the new grid coordinates. While grid metrics and velocities can be computed independently from the actual finite-volume form of the geometric conservation equation, CWC will not be satisfied unless Equation (16) is identically satisfied, and this places constraints on how each of the metrics is computed. For example, if the vertices of a finite-volume, time-dependent grid are given by $(x(t)_{i\pm1/2,j\pm1/2},\ y(t)_{i\pm1/2,j\pm1/2})$, then the cell volume $J^{-1}(t)|_{i,j}$ can be calculated from the grid vertices to second order in space with

$$\begin{aligned} J^{-1}(t)|_{i,j}^{n} &= \left| \begin{matrix} \dfrac{\partial x(t)}{\partial \xi} & \dfrac{\partial x(t)}{\partial \eta} \\ \dfrac{\partial y(t)}{\partial \xi} & \dfrac{\partial y(t)}{\partial \eta} \end{matrix} \right|_{i,j} \\ &\approx \left| \begin{matrix} \dfrac{\delta_\xi x(t)_{i,j+1/2} + \delta_\xi x(t)_{i,j-1/2}}{2} & \dfrac{\delta_\eta x(t)_{i+1/2,j} + \delta_\eta x(t)_{i-1/2,j}}{2} \\ \dfrac{\delta_\xi y(t)_{i,j+1/2} + \delta_\xi y(t)_{i,j-1/2}}{2} & \dfrac{\delta_\eta y(t)_{i+1/2,j} + \delta_\eta y(t)_{i-1/2,j}}{2} \end{matrix} \right| \end{aligned} \tag{17}$$

where $\delta_\xi() = ()_{i+1/2} - ()_{i-1/2}$ and $\delta_\eta() = ()_{j+1/2} - ()_{j-1/2}$. The calculation of the cell volume by Equation (17) assumes the parallelogram shape for each cell in which the edge length in each direction is approximated by the center value in that direction (see Appendix A). However, as shown in Appendix A, in the finite-volume framework, the volume obtained by Equation (17) is not identical to that obtained with a time advancement of Equation (16) while it is identical to that obtained with the finite-difference framework. Thus, in order to ensure geometric conservation with the finite-volume framework and the consistency condition (discussed later), other than the first time step in which $J^{-1}|_{i,j}^{0}$ is obtained with Equation (17), $J^{-1}|_{i,j}^{n+1}$ is updated by integrating in time Equation (16) over the interval $[t^n, t^{n+1}]$ with

$$\begin{aligned} J^{-1}|_{i,j}^{n+1} &= J^{-1}|_{i,j}^{n} + \int_{t^n}^{t^{n+1}} (U_{g,i+1/2,j}(\tau) - U_{g,i-1/2,j}(\tau)) + (V_{g,i,j+1/2}(\tau) - V_{g,i,j-1/2}(\tau))\,\mathrm{d}\tau \\ &= J^{-1}|_{i,j}^{n} + (\widetilde{U}_{g,i+1/2,j} - \widetilde{U}_{g,i-1/2,j})\Delta t + (\widetilde{V}_{g,i,j+1/2} - \widetilde{V}_{g,i,j-1/2})\Delta t \end{aligned} \tag{18}$$

Copyright © 2009 John Wiley & Sons, Ltd.

DOI: 10.1002/fld

where

$$\widetilde{U}=\frac{1}{\Delta t}\int_{t^n}^{t^{n+1}} U(\tau)\,\mathrm{d}\tau$$

and $\Delta t=t^{n+1}-t^n$. In order to ensure a positive cell volume, Equation (18) is subject to the constraints

$$(\widetilde{U}_{g,i+1/2,j}-\widetilde{U}_{g,i-1/2,j})\Delta t>-J^{-1}|^n_{i,j} \quad \text{and} \quad (\widetilde{V}_{g,i,j+1/2}-\widetilde{V}_{g,i,j-1/2})\Delta t>-J^{-1}|^n_{i,j} \tag{19}$$

Violation of condition (19) is the case in which cells overlap and do not share unique vertices. In the case that the coordinates are determined *a priori* at each time step, one can always construct grid points that are uniquely defined in the computational domain, thus satisfying condition (19). This property holds for flow–structure interaction problems in which grid points are determined based on structure behavior at each time step. However, in the case that grids move based on the flowfield, it is possible to violate Equation (19) when the system is strongly nonlinear, such as in shocks. In such a case, as we have mentioned in the introduction, one can employ a grid monitor function to ensure that grid coordinates are always uniquely defined, thus avoiding violation of condition (19). Therefore, in the remainder of this paper, it is reasonable to assume that Equation (19) is always satisfied.

It should be noted that since the cell volume is updated with the finite-volume formulation using Equation (18), discrete geometric conservation is guaranteed both locally and globally, since the summation of Equation (18) over all cells in the domain guarantees that

$$\mathbb{V}_{\mathrm{T}}^{n+1}-\mathbb{V}_{\mathrm{T}}^{n}=\sum_{i,j}(J^{-1}|^{n+1}_{i,j}-J^{-1}|^n_{i,j})=0 \tag{20}$$

where $\mathbb{V}_{\mathrm{T}}^n$ is the total volume of the domain at time step $n$.

### *3.2. GCL in two-dimensional space*

In the previous section, we show how to update the cell volume with the finite-volume formulation, which conserves cell geometry, both locally and globally. However, when Equation (18) is discretized in time, special care must be taken to guarantee discrete conservation of geometry. A simple example is shown in Figure 2 to illustrate this issue, which arises when Equation (18) is fully discretized in multi-dimensional space. In order to demonstrate this in a more general sense, we rewrite the contravariant volume fluxes ($U$, $V$) in a two-dimensional computational domain ($\xi$, $\eta$) as

$$U=\frac{\partial y}{\partial \eta}u-\frac{\partial x}{\partial \eta}v \quad \text{and} \quad V=-\frac{\partial y}{\partial \xi}u+\frac{\partial x}{\partial \xi}v \tag{21}$$

Equation (16) can thus be rewritten as

$$\begin{aligned}\frac{\mathrm{d}}{\mathrm{d}t}(J^{-1}|_{i,j})=&\left(\frac{\partial y}{\partial \eta}u_g-\frac{\partial x}{\partial \eta}v_g\right)_{i+1/2,j}-\left(\frac{\partial y}{\partial \eta}u_g-\frac{\partial x}{\partial \eta}v_g\right)_{i-1/2,j}\\&+\left(-\frac{\partial y}{\partial \xi}u_g+\frac{\partial x}{\partial \xi}v_g\right)_{i,j+1/2}-\left(-\frac{\partial y}{\partial \xi}u_g+\frac{\partial x}{\partial \xi}v_g\right)_{i,j-1/2}\end{aligned} \tag{22}$$

Copyright © 2009 John Wiley & Sons, Ltd.

DOI: 10.1002/fld

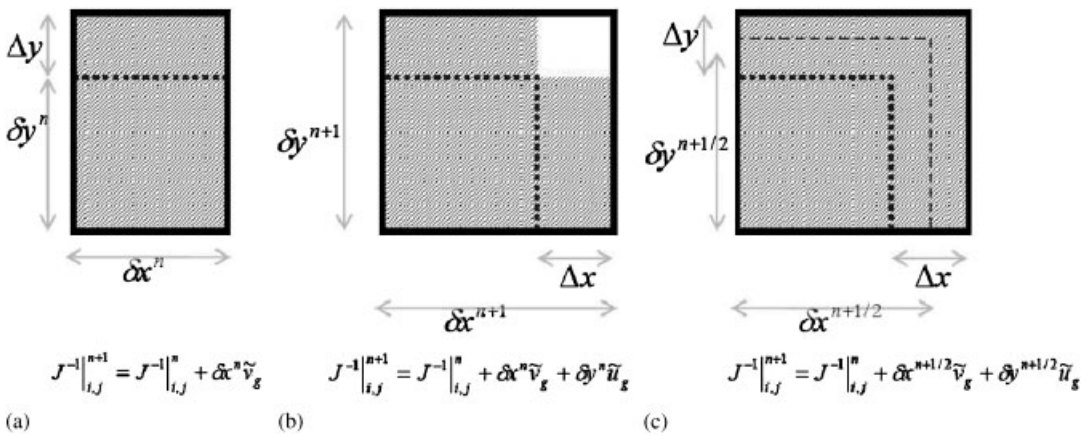


Figure 2. Depiction of grid deformation in: (a) one dimension and (b, c) two dimensions, in which the dotted thick lines indicate the edges of the old cell while the solid thick lines indicate edges of the new cell. The shaded area is the cell volume (area) calculated from the equation below it. This illustrates that in the 1-D case, the new cell volume (area) can be directly updated using the grid velocity, but in the 2-D case, the intermediate edge length, $\delta x^{n+1/2}$ and $\delta y^{n+1/2}$, must be used in order to obtain the actual volume change.

where the first two terms on the right-hand side correspond to the volume change due to grid motion in the $\xi$-direction, while the last two terms correspond to the volume change due to grid motion in the $\eta$-direction. All terms in Equation (22) are time-dependent, and the metric quantities in this equation (e.g. $\partial x/\partial\xi$) represent the face lengths associated with the respective normal grid velocities in each curvilinear coordinate direction ($\xi$, $\eta$). These metrics are exact at each time step because the faces of the finite-volume cells are assumed to be linear.

Consider the assumption of a constant grid velocity field ($U^n_{g,i,j}$, $V^n_{g,i,j}$) between $t=t^n$ and $t^{n+1}$, which has been done in numerous related studies (e.g. [20–22]). Under this assumption, the forward Euler (FE) discretization of (16) is given by

$$J^{-1}|_{i,j}^{n+1} = J^{-1}|_{i,j}^{n} + \Delta t\,(U^n_{g,i+1/2,j} - U^n_{g,i-1/2,j}) + \Delta t\,(V^n_{g,i,j+1/2} - V^n_{g,i,j-1/2}) \tag{23}$$

As all terms on the right-hand side of Equation (23) are calculated at time step $n$, geometry is not conserved since the real volume change of each cell $\Delta J^{-1}|_{i,j}^{n} = J^{-1}|_{i,j}^{n+1} - J^{-1}|_{i,j}^{n}$ is not equal to the RHS of Equation (23). As illustrated in Figures 2(a) and (b), the difference between one- and two-dimensional grid movement is that, in the two-dimensional case, the actual area change of each cell should include the area change $(U_{g,i,j}\Delta t)\times(V_{g,i,j}\Delta t)$, which is omitted if Equation (23) is employed. This geometric conservation issue associated with multi-dimensional moving-grid simulations has been addressed by Demirdzic and Peric [19], and they proposed an alternative grid velocity to satisfy conservation of cell geometry, which is given by (in the $x$–$y$ plane)

$$u_g = \frac{\delta y^{n+1} + \delta y^n}{2\delta y^n}\frac{\Delta x}{\Delta t} \quad \text{and} \quad v_g = \frac{\delta x^{n+1} + \delta x^n}{2\delta x^n}\frac{\Delta y}{\Delta t} \tag{24}$$

Copyright © 2009 John Wiley & Sons, Ltd.

DOI: 10.1002/fld

such that changes in cell geometry are given identically by

$$\Delta J = (\delta y^n u_g + \delta x^n v_g)\Delta t \tag{25}$$

which conserves grid geometry when the grid moves in two-dimensional space. One alternative approach to solving this problem is to employ the operator splitting scheme, in which the cell volume is updated in different coordinate directions subsequently at each time step. Although the formulation for the cell volume update can maintain the actual cell volume with operator splitting, the splitting procedure for physical scalar transport would result in violation of the consistency condition, as demonstrated by Leonard *et al.* [4]. As an example, the splittling procedure for a scalar field ($C_{i,j}$) in the $x$–$y$ plane is written as

$$\begin{aligned} C^*_{i,j} &= C^n_{i,j} + u^n_{i-1/2,j} C^n_{i-1/2,j} - u^n_{i+1/2,j} C^n_{i+1/2,j} \\ C^{n+1}_{i,j} &= C^*_{i,j} + v^n_{i,j-1/2} C^*_{i,j-1/2} - v^n_{i,j+1/2} C^*_{i,j+1/2} \end{aligned} \tag{26}$$

Assuming a constant concentration field $S$ in space, this becomes

$$\begin{aligned} S^* &= S^n + u^n_{i-1/2,j} S^n - u^n_{i+1/2,j} S^n \\ S^{n+1} &= S^* + v^n_{i,j-1/2} S^* - v^n_{i,j+1/2} S^* \end{aligned} \tag{27}$$

and combining these two equations together to eliminate the intermediate value $S^*$ results in

$$\begin{aligned} S^{n+1} = S^n &+ (u^n_{i-1/2,j} - u^n_{i+1/2,j} + v^n_{i-1/2,j} - v^n_{i+1/2,j}) S^n \\ &+ (u^n_{i-1/2,j} v^n_{i,j-1/2} - u^n_{i+1/2,j} v^n_{i,j+1/2} - u^n_{i-1/2,j} v^n_{i,j+1/2} + u^n_{i+1/2,j} v^n_{i,j-1/2}) S^n \end{aligned} \tag{28}$$

The CWC condition requires that $S^{n+1} = S^n$ throughout the simulation. Since the second term on the RHS of Equation (28) is zero due to continuity, the only way to ensure CWC is if the third term on the RHS is identically zero. However, in general this is not true, thus violating CWC. Since the splitting procedure in $m$ dimensions requires $m-1$ intermediate solutions, splitting is also not desirable when higher-order multi-step methods are employed.

In this study, to maintain GCL and to avoid the problems associated with operator splitting, we employ a cell volume updating procedure that uses intermediate metric quantities to approximate the volume change. Since the metric quantities are exact at each time step because the finite-volume faces are linear and the coordinates of the finite-volume vertices at the new time step are known *a priori*, we use the intermediate metric quantities, which are defined by the average of the metrics at time step $n$ and time step $n+1$. As an example, for $\partial x/\partial \xi$ we use

$$\left.\frac{\partial x}{\partial \xi}\right|^{n+1/2} = \frac{1}{2}\left( \left.\frac{\partial x}{\partial \xi}\right|^{n} + \left.\frac{\partial x}{\partial \xi}\right|^{n+1} \right) \tag{29}$$

The components of the grid velocity ($u_g$, $v_g$) for each cell are calculated from the movement of the mid-point of each face ($(\Delta x, \Delta y)_{i\pm 1/2,j \text{ or } i,j\pm 1/2}$), which is computed via an average of the movement of the end points of each face. Using these assumptions, if a constant grid velocity is assumed between $t = t^n$ and $t^{n+1}$ for each cell face, then Equation (18) becomes

$$J^{-1}|^{n+1}_{i,j} = J^{-1}|^{n}_{i,j} + \Delta t (U^{n+1/2,n}_{g,i+1/2,j} - U^{n+1/2,n}_{g,i-1/2,j}) + \Delta t (V^{n+1/2,n}_{g,i,j+1/2} - V^{n+1/2,n}_{g,i,j-1/2}) \tag{30}$$

Copyright © 2009 John Wiley & Sons, Ltd.

DOI: 10.1002/fld

where

$$U^{n+1/2,n}_{g,i\pm1/2,j} = \left.\frac{\partial y}{\partial \eta}\right|^{n+1/2}_{i\pm1/2,j} u^n_{g,i\pm1/2,j} - \left.\frac{\partial x}{\partial \eta}\right|^{n+1/2}_{i\pm1/2,j} v^n_{g,i\pm1/2,j} \tag{31}$$

and

$$V^{n+1/2,n}_{g,i,j\pm1/2} = -\left.\frac{\partial y}{\partial \xi}\right|^{n+1/2}_{i,j\pm1/2} u^n_{g,i,j\pm1/2} + \left.\frac{\partial x}{\partial \xi}\right|^{n+1/2}_{i,j\pm1/2} v^n_{g,i,j\pm1/2} \tag{32}$$

and the Cartesian grid velocities in Equations (31) and (32) are given by

$$\begin{aligned} u_{g,i\pm1/2,j} &= \frac{\Delta x|_{i\pm1/2,j}}{\Delta t}, \quad v_{g,i\pm1/2,j} = \frac{\Delta y|_{i\pm1/2,j}}{\Delta t} \\ u_{g,i,j\pm1/2} &= \frac{\Delta x|_{i,j\pm1/2}}{\Delta t}, \quad v_{g,i,j\pm1/2} = \frac{\Delta y|_{i,j\pm1/2}}{\Delta t} \end{aligned} \tag{33}$$

The difference between Equations (23) and (30) is illustrated in Figure 2. Both the present formulation (Equations (30)–(33)) and those of Demirdzic and Peric [19] (Equations (24) and (25)) conserve grid geometry, but the associated Cartesian grid velocities (Equations (24) and (33)) are different. In the present study, the use of the intermediate metric quantities (Equation (29)) eliminates the dependence of the approximated grid velocity on grid geometry, which can be demonstrated by comparing Equations (24) and (33). Moreover, Equations (30)–(33) can easily be extended to three dimensions (see Appendix B).

In order to distinguish between the metric and physical quantities, we introduce the geometric operator $\mathbf{G}^n_{\xi,i,j}(\cdot)$ which represents the metric quantity evaluated at location $(i, j)$ in the $\xi$-direction at time step $t = t^n$. For example,

$$\mathbf{G}^{n+1/2}_{\xi,i+1/2,j}(u^n C^n) = \left.\frac{\partial \xi}{\partial x}\right|^{n+1/2}_{i+1/2} (uC)^n_{i+1/2,j} + \left.\frac{\partial \xi}{\partial y}\right|^{n+1/2}_{i+1/2,j} (vC)^n_{i+1/2,j} = U^{n+1/2,n}_{i+1/2,j} C^n_{i+1/2,j} \tag{34}$$

and Equation (30) can thus be rewritten as

$$\begin{aligned} J^{-1}|^{n+1}_{i,j} = J^{-1}|^n_{i,j} &+ \Delta t(\mathbf{G}^{n+1/2}_{\xi,i+1/2,j}(u^n_g) - \mathbf{G}^{n+1/2}_{\xi,i-1/2,j}(u^n_g)) \\ &+ \Delta t(\mathbf{G}^{n+1/2}_{\eta,i,j+1/2}(v^n_g) - \mathbf{G}^{n+1/2}_{\eta,i,j-1/2}(v^n_g)) \end{aligned} \tag{35}$$

Unlike Equation (23), this equation ensures geometric conservation both locally and globally.

## 4. CONSISTENT DISCRETIZATION OF SCALAR TRANSPORT

In Section 2.2, finite-volume discretizations were formulated for the conservation laws of scalar and fluid in Equations (13) and (14), respectively. The face values in these equations can be obtained from different interpolation schemes depending on the desired numerical properties, and mass conservation for both fluid and scalar can be achieved in a straightforward manner. In a fixed-grid simulation, $\partial J^{-1}/\partial t = 0$ and $u_{g,i,j} = 0$, and CWC is satisfied as long as, if the simulation is started with an initial constant in space, the interpolation scheme that is used to interpolate face

Copyright © 2009 John Wiley & Sons, Ltd.

DOI: 10.1002/fld

values in Equation (13) yields the same constant at each cell face during the simulation. This can be demonstrated by substituting a constant concentration field into Equation (13), and the result is the discrete continuity equation

$$(U_{i+1/2,j}-U_{i-1/2,j})+(V_{i,j+1/2}-V_{i,j-1/2})=0 \tag{36}$$

which, for the moving-grid case, can be written as

$$(\mathbf{G}^{n+1/2}_{\xi,i+1/2,j}(u^n)-\mathbf{G}^{n+1/2}_{\xi,i-1/2,j}(u^n))+(\mathbf{G}^{n+1/2}_{\eta,i,j+1/2}(v^n)-\mathbf{G}^{n+1/2}_{\eta,i,j-1/2}(v^n))=0 \tag{37}$$

It is important to note that grid motion is not necessarily dependent on fluid motion and can be prescribed exactly prior to each time step, and the method by which it is calculated can conserve grid geometry as was demonstrated in Section 3. Therefore, there is no stability constraint arising from the discretization scheme for the GCL (Equation (16)) as long as constraint (19) is satisfied. However, a stable discretization of the GCL that conserves grid geometry constrains the temporal discretization of the scalar transport Equation (13), since the same temporal discretization technique that is used for the discrete GCL must be used for scalar transport if CWC is to be achieved. In what follows, we discuss examples of different consistent discretization techniques applied to the GCL (16) and the transport Equation (13).

### *4.1. First-order forward Euler method*

If Equation (35) is used to update the cell volume, CWC is satisfied only if the forward Euler (FE) method is used as the temporal discretization for the scalar transport equation. That is, Equation (13) must be discretized as

$$\begin{aligned} J^{-1}|^{n+1}_{i,j}C^{n+1}_{i,j} = J^{-1}|^{n}_{i,j}C^{n}_{i,j} &-\Delta t(\mathbf{G}^{n+1/2}_{\xi,i+1/2,j}(u^nC^n)-\mathbf{G}^{n+1/2}_{\xi,i-1/2,j}(u^nC^n))\\ &-\Delta t(\mathbf{G}^{n+1/2}_{\xi,i,j+1/2}(v^nC^n)-\mathbf{G}^{n+1/2}_{\xi,i,j-1/2}(v^nC^n))\\ &+\Delta t(\mathbf{G}^{n+1/2}_{\eta,i+1/2,j}(u^n_gC^n)-\mathbf{G}^{n+1/2}_{\eta,i+1/2,j}(u^n_gC^n))\\ &+\Delta t(\mathbf{G}^{n+1/2}_{\eta,i,j+1/2}(v^n_gC^n)-\mathbf{G}^{n+1/2}_{\eta,i,j-1/2}(v^n_gC^n)) \end{aligned} \tag{38}$$

CWC can be demonstrated by substituting the constant concentration field $C_{i,j}=1$ into Equation (38), and subtracting Equation (35), which yields Equation (37). Although this discretization is consistent, the temporal accuracy is only first order. To improve the temporal accuracy, one can employ the second-order Adams–Bashforth (AB2) method to discretize Equation (13). However, because the first-order approximation

$$u_{g,i,j}=\frac{x^{n+1}_{i,j}-x^n_{i,j}}{\Delta t}+\mathcal{O}(\Delta t)\quad\text{and}\quad v_{g,i,j}=\frac{y^{n+1}_{i,j}-y^n_{i,j}}{\Delta t}+\mathcal{O}(\Delta t) \tag{39}$$

is employed for the grid velocity, the terms associated with the grid velocity in the scalar transport equation must also be discretized in time using the FE method. The resulting discrete scalar

Copyright © 2009 John Wiley & Sons, Ltd.

DOI: 10.1002/fld

transport equation is given by

$$
\begin{aligned}
J^{-1}|_{i,j}^{n+1} C_{i,j}^{n+1} = J^{-1}|_{i,j}^{n} C_{i,j}^{n} &- \Delta t[\tfrac{3}{2}(\mathbf{G}_{\xi,i+1/2,j}^{n+1/2}(u^n C^n) - \mathbf{G}_{\xi,i-1/2,j}^{n+1/2}(u^n C^n)) \\
&- \tfrac{1}{2}(\mathbf{G}_{\xi,i+1/2,j}^{n+1/2}(u^{n-1} C^{n-1}) - \mathbf{G}_{\xi,i-1/2,j}^{n+1/2}(u^{n-1} C^{n-1}))] \\
&- \Delta t[\tfrac{3}{2}(\mathbf{G}_{\eta,i,j+1/2}^{n+1/2}(v^n C^n) - \mathbf{G}_{\eta,i,j-1/2}^{n+1/2}(v^n C^n)) \\
&- \tfrac{1}{2}(\mathbf{G}_{\eta,i,j+1/2}^{n+1/2}(v^{n-1} C^{n-1}) - \mathbf{G}_{\eta,i,j-1/2}^{n+1/2}(v^{n-1} C^{n-1}))] \\
&+ \Delta t(\mathbf{G}_{\xi,i+1/2,j}^{n+1/2}(u_g^n C^n) - \mathbf{G}_{\xi,i+1/2,j}^{n+1/2}(u_g^n C^n)) \\
&+ \Delta t(\mathbf{G}_{\eta,i,j+1/2}^{n+1/2}(v_g^n C^n) - \mathbf{G}_{\eta,i,j-1/2}^{n+1/2}(v_g^n C^n))
\end{aligned} \tag{40}
$$

Since the higher-order temporal discretization is employed for the transport associated with the physical velocity ($u$, $v$), the temporal accuracy is improved, but due to the grid transport terms (containing $u_g$, $v_g$), Equation (40) is still first-order accurate in time. However, this is necessary for CWC because any discretization other than FE for the grid transport terms in the scalar transport equation would violate consistency. Violation of CWC can be demonstrated by discretizing the grid transport terms in Equation (40) with AB2. Applying a constant concentration field and subtracting Equation (37) yields

$$
\begin{aligned}
J^{-1}|_{i,j}^{n+1} = J^{-1}|_{i,j}^{n} &+ \Delta t[\tfrac{3}{2}(\mathbf{G}_{\xi,i+1/2,j}^{n+1/2}(u_g^n) - \mathbf{G}_{\xi,i-1/2,j}^{n+1/2}(u_g^n)) \\
&- \tfrac{1}{2}(\mathbf{G}_{\xi,i+1/2,j}^{n+1/2}(u_g^{n-1}) - \mathbf{G}_{\xi,i-1/2,j}^{n+1/2}(u_g^{n-1}))] \\
&+ \Delta t[\tfrac{3}{2}(\mathbf{G}_{\eta,i,j+1/2}^{n+1/2}(v_g^n) - \mathbf{G}_{\eta,i,j-1/2}^{n+1/2}(v_g^n)) \\
&- \tfrac{1}{2}(\mathbf{G}_{\eta,i,j+1/2}^{n+1/2}(v_g^{n-1}) - \mathbf{G}_{\eta,i,j-1/2}^{n+1/2}(v_g^{n-1}))]
\end{aligned} \tag{41}
$$

which is not identical to Equation (35), and would induce excessive mass creation during the simulation if the grid is updated with Equation (35). We can conclude that, since a first-order approximation is assumed for the grid velocity, high-order temporal accuracy is not attainable for scalar transport without violating CWC.

### *4.2. Second-order Adams–Bashforth method*

Second-order temporal accuracy for grid movement can be achieved if the grid volume is updated with Equation (41) and, based on the AB2 method, a second-order accurate approximation for the grid velocity is given by

$$
\begin{aligned}
u_{g,i,j}^n &= \frac{2}{3}\frac{x_{i,j}^{n+1} - x_{i,j}^n}{\Delta t} + \frac{1}{3}u_{g,i,j}^{n-1} + \mathcal{O}(\Delta t^2) \\
v_{g,i,j}^n &= \frac{2}{3}\frac{y_{i,j}^{n+1} - y_{i,j}^n}{\Delta t} + \frac{1}{3}v_{g,i,j}^{n-1} + \mathcal{O}(\Delta t^2)
\end{aligned} \tag{42}
$$

Copyright © 2009 John Wiley & Sons, Ltd.

DOI: 10.1002/fld

Using Equations (41) and (42), the temporal accuracy of the moving-grid simulation can be improved to second order, and the associated consistent discretization of the scalar transport Equation (13) is given by

$$
\begin{aligned}
J^{-1}|_{i,j}^{n+1} C_{i,j}^{n+1} = J^{-1}|_{i,j}^{n} C_{i,j}^{n} &- \Delta t[\tfrac{3}{2}(\mathbf{G}_{\xi,i+1/2,j}^{n+1/2}(u^n C^n) - \mathbf{G}_{\xi,i-1/2,j}^{n+1/2}(u^n C^n)) \\
&- \tfrac{1}{2}(\mathbf{G}_{\xi,i+1/2,j}^{n+1/2}(u^{n-1} C^{n-1}) - \mathbf{G}_{\xi,i-1/2,j}^{n+1/2}(u^{n-1} C^{n-1}))] \\
&- \Delta t[\tfrac{3}{2}(\mathbf{G}_{\eta,i,j+1/2}^{n+1/2}(v^n C^n) - \mathbf{G}_{\eta,i,j-1/2}^{n+1/2}(v^n C^n)) \\
&- \tfrac{1}{2}(\mathbf{G}_{\eta,i,j+1/2}^{n+1/2}(v^{n-1} C^{n-1}) - \mathbf{G}_{\eta,i,j-1/2}^{n+1/2}(v^{n-1} C^{n-1}))] \\
&+ \Delta t[\tfrac{3}{2}(\mathbf{G}_{\xi,i+1/2,j}^{n+1/2}(u_g^n C^n) - \mathbf{G}_{\xi,i-1/2,j}^{n+1/2}(u_g^n C^n)) \\
&- \tfrac{1}{2}(\mathbf{G}_{\xi,i+1/2,j}^{n+1/2}(u_g^{n-1} C^{n-1}) - \mathbf{G}_{\xi,i-1/2,j}^{n+1/2}(u_g^{n-1} C^{n-1}))] \\
&+ \Delta t[\tfrac{3}{2}(\mathbf{G}_{\eta,i,j+1/2}^{n+1/2}(v_g^n C^n) - \mathbf{G}_{\eta,i,j-1/2}^{n+1/2}(v_g^n C^n)) \\
&- \tfrac{1}{2}(\mathbf{G}_{\eta,i,j+1/2}^{n+1/2}(v_g^{n-1} C^{n-1}) - \mathbf{G}_{\eta,i,j-1/2}^{n+1/2}(v_g^{n-1} C^{n-1}))]
\end{aligned} \tag{43}
$$

It is straightforward to show that the substitution of a constant concentration field into Equation (43) yields Equation (41) after subtraction of Equation (37), thereby proving CWC.

Although CWC is achieved in Equation (43), the discretization incurs significant computational overhead when compared with a typical non-CWC discretization. Consider the naive AB2 discretization of Equation (13), which gives

$$
\begin{aligned}
J^{-1}|_{i,j}^{n+1} C_{i,j}^{n+1} = J^{-1}|_{i,j}^{n} C_{i,j}^{n} &- \Delta t[\tfrac{3}{2}((U^n C^n)_{i+1/2,j} - (U^n C^n)_{i-1/2,j}) \\
&- \tfrac{1}{2}((U^{n-1} C^{n-1})_{i+1/2,j} - (U^{n-1} C^{n-1})_{i-1/2,j})] \\
&- \Delta t[\tfrac{3}{2}((V^n C^n)_{i,j+1/2} - (V^n C^n)_{i,j+1/2}) \\
&- \tfrac{1}{2}((V^{n-1} C^{n-1})_{i,j+1/2} - (V^{n-1} C^{n-1})_{i,j-1/2})] \\
&+ \Delta t[\tfrac{3}{2}((U_g^n C^n)_{i+1/2,j} - (U_g^n C^n)_{i-1/2,j}) \\
&- \tfrac{1}{2}((U_g^{n-1} C^{n-1})_{i+1/2,j} - (U_g^{n-1} C^{n-1})_{i-1/2,j})] \\
&+ \Delta t[\tfrac{3}{2}((V_g^n C^n)_{i,j+1/2} - (V_g^n C^n)_{i,j+1/2}) \\
&- \tfrac{1}{2}((V_g^{n-1} C^{n-1})_{i,j+1/2} - (V_g^{n-1} C^{n-1})_{i,j-1/2})]
\end{aligned} \tag{44}
$$

where the metrics and velocities used to compute the contravariant volume fluxes $U$ and $V$ are concurrent in time. Although second-order accurate in time, this discretization is not CWC because substitution of $C_{i,j} = 1$ does not yield Equation (41) after subtraction of Equation (37). Furthermore, replacing Equation (41) with the discrete GCL that results from Equation (44) upon substitution of $C_{i,j} = 1$ does not conserve grid geometry. However, Equation (44) does yield

Copyright © 2009 John Wiley & Sons, Ltd.

DOI: 10.1002/fld

substantial computational savings over Equation (43) because the contravariant mass fluxes ($UC$ and $VC$) on the faces can be stored to form the terms on the right-hand side that are evaluated at time $t^{n-1}$ in Equation (44). This is not possible in Equation (43), because the metric quantities (i.e. $\mathbf{G}()$) are always evaluated at time $t^{n+1/2}$ and therefore the terms containing quantities at time $t^{n-1}$ must be re-evaluated at each time step. Computational savings can be achieved in Equation (43) if the metrics that are used to evaluate the terms at $t^{n-1}$ are evaluated at time $t^{n-1/2}$ rather than at time $t^{n+1/2}$, such that Equation (43) would be given by

$$
\begin{aligned}
J^{-1}|_{i,j}^{n+1} C_{i,j}^{n+1} = J^{-1}|_{i,j}^{n} C_{i,j}^{n} &- \Delta t[\tfrac{3}{2}(\mathbf{G}_{\xi,i+1/2,j}^{n+1/2}(u^n C^n) - \mathbf{G}_{\xi,i-1/2,j}^{n+1/2}(u^n C^n)) \\
&- \tfrac{1}{2}(\mathbf{G}_{\xi,i+1/2,j}^{n-1/2}(u^{n-1} C^{n-1}) - \mathbf{G}_{\xi,i-1/2,j}^{n-1/2}(u^{n-1} C^{n-1}))] \\
&- \Delta t[\tfrac{3}{2}(\mathbf{G}_{\eta,i,j+1/2}^{n+1/2}(v^n C^n) - \mathbf{G}_{\eta,i,j-1/2}^{n+1/2}(v^n C^n)) \\
&- \tfrac{1}{2}(\mathbf{G}_{\eta,i,j+1/2}^{n-1/2}(v^{n-1} C^{n-1}) - \mathbf{G}_{\eta,i,j-1/2}^{n-1/2}(v^{n-1} C^{n-1}))] \\
&+ \Delta t[\tfrac{3}{2}(\mathbf{G}_{\xi,i+1/2,j}^{n+1/2}(u_g^n C^n) - \mathbf{G}_{\xi,i-1/2,j}^{n+1/2}(u_g^n C^n)) \\
&- \tfrac{1}{2}(\mathbf{G}_{\xi,i+1/2,j}^{n-1/2}(u_g^{n-1} C^{n-1}) - \mathbf{G}_{\xi,i-1/2,j}^{n-1/2}(u_g^{n-1} C^{n-1}))] \\
&+ \Delta t[\tfrac{3}{2}(\mathbf{G}_{\eta,i,j+1/2}^{n+1/2}(v_g^n C^n) - \mathbf{G}_{\eta,i,j-1/2}^{n+1/2}(v_g^n C^n)) \\
&- \tfrac{1}{2}(\mathbf{G}_{\eta,i,j+1/2}^{n-1/2}(v_g^{n-1} C^{n-1}) - \mathbf{G}_{\eta,i,j-1/2}^{n-1/2}(v_g^{n-1} C^{n-1}))]
\end{aligned} \tag{45}
$$

Although this discretization does not satisfy CWC exactly, it eliminates the number of operations by a factor of two relative to the CWC version given by Equation (43), and CWC is only slightly violated as long as it is assumed that the grid motion is small.

## 5. NUMERICAL EXAMPLES

### *5.1. Example 1: test of temporal accuracy and convergence rate*

Here, we present a simple test case to demonstrate transport due to a moving grid. In this case, the velocity field is zero everywhere throughout the simulation and the scalar field is only affected by the grid velocity. We simulate the transport equation derived from the aforementioned conservation law without considering physical diffusion. This is designed to test the accuracy and consistency of the proposed moving-grid algorithm which we apply to the curvilinear coordinate Navier–Stokes code originally developed by Zang *et al.* [17] and parallelized by Cui and Street [23]. The simulation is conducted in a three-dimensional cubic domain with $x \in [0, L]$, $y \in [0, W]$, and $z \in [-D, 0]$, with $L = W = H$, where $z$ is the vertical coordinate and a grid resolution of $32 \times 32 \times 32$

Copyright © 2009 John Wiley & Sons, Ltd.

DOI: 10.1002/fld

is employed. Given a uniformly distributed coordinate system $x_0 \in [0, 1]$, $y_0 \in [0, 1]$, and $z_0 \in [0, 1]$, the coordinates of the grid points in the solution domain are obtained through the mapping function

$$x_{i,j} = L\left(\frac{\exp(a_x x_{0,i,j})-1}{\exp(a_x)-1}\right), \quad y_{i,j} = W\left(1-\frac{\exp(a_y y_{0,i,j})-1}{\exp(a_y)-1}\right)$$
$$z_{i,j} = -H\left(1-\frac{\exp(a_z z_{0,i,j})-1}{\exp(a_z)-1}\right) \tag{46}$$

where $a_x = 1+\sin[2\pi(z_{0,i,j}+t/T)]$, $a_y = 1+\sin[2\pi(z_{0,i,j}+t/T)]$, and $a_z = 1+\cos[4\pi(x_{i,j}/L+t/T)]+\cos[4\pi(y_{i,j}/W+t/T)]$. Using this mapping, the grid is distorted in the $\xi$-, $\eta$-, and $\zeta$-directions and moves periodically with period $T$. In order to study the influence of using a non-CWC discretization and the effects of the temporal accuracy on CWC (or lack thereof) in a simulation in which only the grid moves and the flow remains static, we simulate different initial conditions using the grid defined by Equation (46) using three different configurations. In case I, a consistent discretization is employed by using AB2 for both scalar transport (Equation (43)) and the GCL (Equation (41)), while in case II a consistent discretization is employed by using FE for both (Equations (38) and (35), respectively). To ensure the desired accuracy, case I employs AB2 for the grid velocity (Equation (42)), while case II employs FE (Equation (39)). In case III, the scalar transport equation is discretized using AB2 (Equation (43)), but the GCL and grid velocities are discretized using FE (Equations (35) and (39), respectively), thereby violating CWC. The computational grid at representative time steps over one period $T$ is shown in Figure 3, which demonstrates pronounced three-dimensional grid skewness.

We first demonstrate the difference between CWC and non-CWC cases by starting from a constant concentration field ($C = 1.0$) in cases I and III. The simulation time step is $\Delta t = 0.0025T$, yielding a Courant–Friedrichs–Lewy (CFL) number of roughly 0.35 throughout the simulation, where the CFL number is calculated with

$$\mathrm{CFL} = \mathrm{Max}_{i,j}\left[\left|\frac{u_{i,j}-u_{g,i,j}}{\Delta x}+\frac{v_{i,j}-v_{g,i,j}}{\Delta y}+\frac{w_{i,j}-w_{g,i,j}}{\Delta z}\right|\right]\Delta t \tag{47}$$

The concentration fields at representative time steps over one simulation period are shown in Figure 3, which demonstrates that the CWC case is able to preserve the constant scalar field while the non-CWC case fails to do so. This is because of the violation of mass conservation due to the inconsistency of the discretization between the continuity equation and the scalar transport equation.

In addition to studying the effects of a non-consistent discretization, we also compare the temporal convergence rates for cases I and II to show that the CWC methods described in this paper ensure the desired temporal accuracy. The aforementioned simulation setup is used but with a different initial condition given by

$$S_{0,i,j} = 0.5-0.1\tanh\left[\frac{2\sqrt{(x_{i,j}-0.25)^2+(y_{i,j}-0.25)^2+(z_{i,j}+0.25)^2}-0.1}{0.05}\right] \tag{48}$$

The time step sizes we use for comparison are $\Delta t = 0.004T$, $0.002T$, $0.001T$, and $0.0005T$, such that the maximum CFL number is about 0.3 when $\Delta t = 0.004T$. In order to obtain the convergence

Copyright © 2009 John Wiley & Sons, Ltd.

DOI: 10.1002/fld

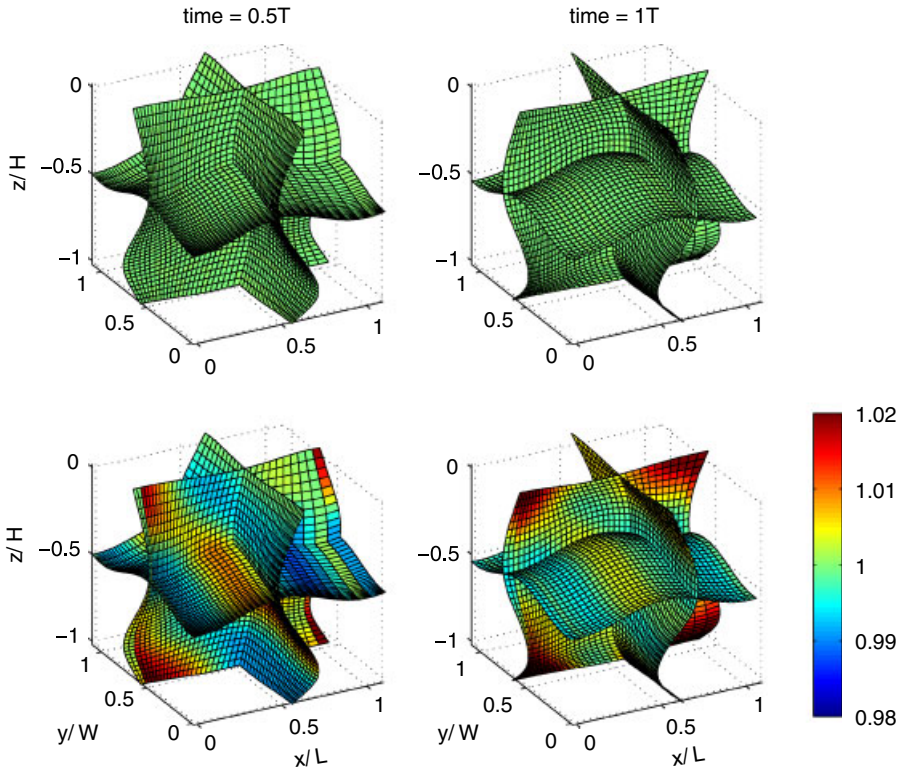


Figure 3. Snapshots of three-dimensional periodic, highly skewed grid deformation superimposed with concentration plots starting from a constant concentration field ($C_0 = 1.0$) at certain time steps from the CWC case (case I, top) and the non-CWC case (case III, bottom).

rate, we use a reference value for the error calculation, such that

$$\text{ERROR}_{\text{ref}} = \sqrt{\frac{\sum_{i,j}(S_{i,j} - S_{\text{ref},i,j})J^{-1}|_{i,j}}{\sum_{i,j} S_{\text{ref},i,j} J^{-1}|_{i,j}}} \tag{49}$$

where the reference solution of the concentration field $S_{\text{ref},i,j}$ and the cell volume $J^{-1}|_{i,j}$ are obtained from a simulation using a time step size of $\Delta t = 0.00025T$. The resulting errors with different $\Delta t$ are plotted in Figure 4, which shows good agreement between our results and the theoretical convergence rates.

### 5.2. *Example 2: moving boundary*

As a second example, we simulate a flowfield resulting from a moving boundary. In this example, the velocity field is initially quiescent and the flow is induced by a no-slip condition on the bed at the bottom boundary, such that, if $h$ represents the departure of the bed from its initial horizontal

Copyright © 2009 John Wiley & Sons, Ltd.

DOI: 10.1002/fld

orientation, then the motion of the bed is given by

$$\frac{h}{H} = -\frac{a}{H}\cos\left[\frac{2\pi}{\lambda}(x+0.25)\right]\sin\left(\frac{2\pi t}{T}\right) \tag{50}$$

where $H$ is the mean height of the domain, the oscillation amplitude is $a=0.067H$, the wavelength is $\lambda=0.5L$, and the period is $T$. The domain size is $L\times W\times H$ with $W=0.2L$ and $H=0.6L$, and a grid resolution of $80\times 16\times 64$ is employed. The grid is stretched in the vertical direction, resulting

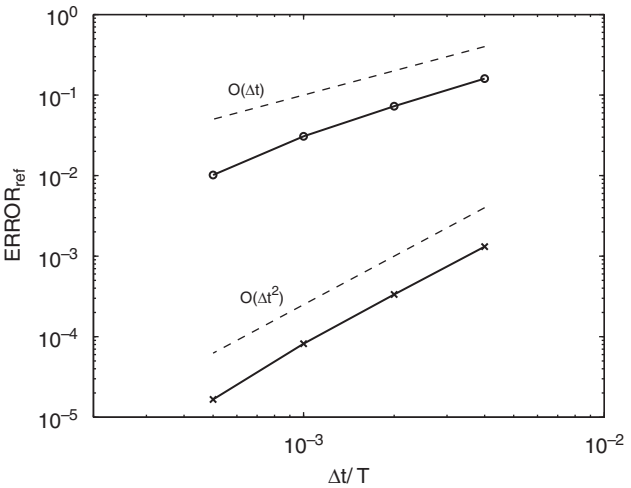


Figure 4. Temporal convergence results of the concentration field for the grid velocity calculated using the first-order method in case II (○) and the second-order method in case I (×) along with theoretical slopes shown by dashed lines.

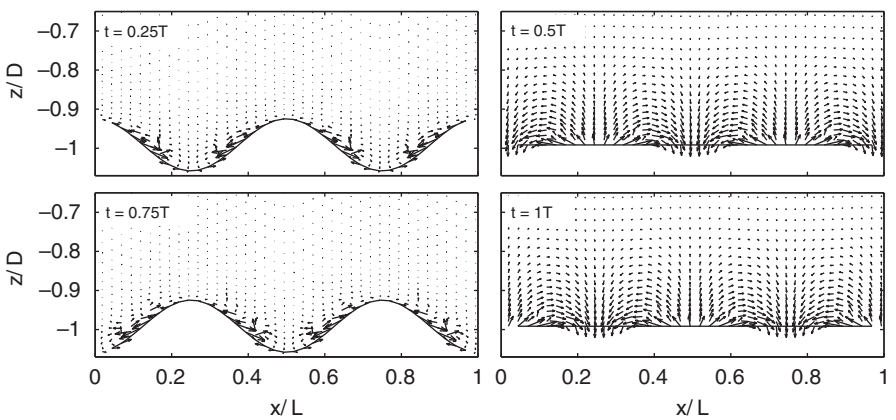


Figure 5. Snapshots of the flow field, shown by arrows, induced by the oscillatory boundary for the simulation of flow over a moving boundary.

Copyright © 2009 John Wiley & Sons, Ltd.

DOI: 10.1002/fld

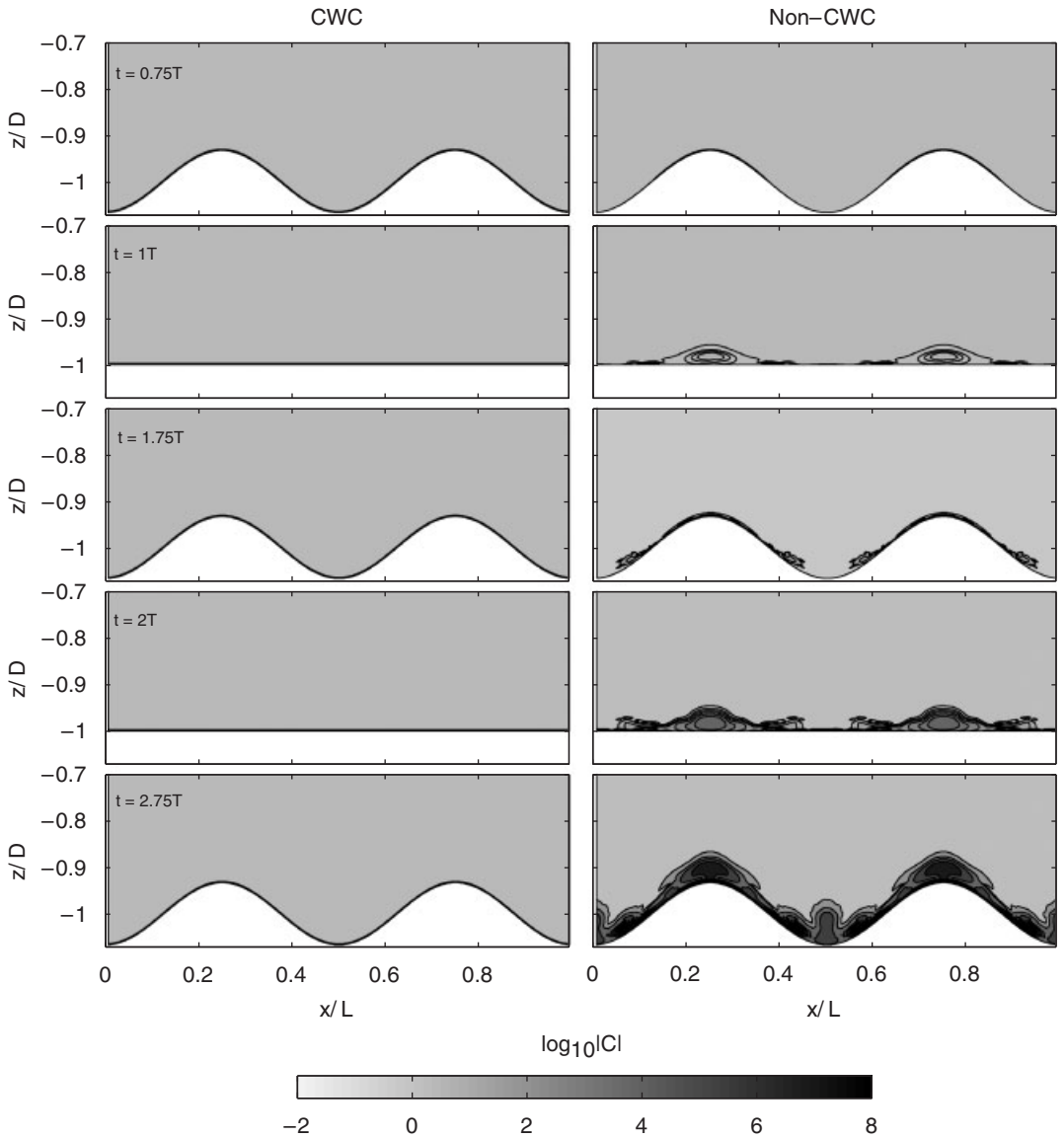


Figure 6. Time evolution of an initially uniform scalar field $C = 1$ and the effects of using a CWC method (left column) and a non-CWC method (right column).

in a vertical grid spacing $\Delta z$ ranging from $0.002L$ (the bottom cell) to $0.01L$ (the top cell). The total simulation time is $3T$ and the time step is $\Delta t = 0.002T$, yielding a maximum CFL number of roughly 0.15, and momentum and scalar transport, along with the GCL, are computed with the AB2 method (as in case I above). The velocity field induced by the moving bed is depicted in Figure 5. A uniform scalar field $C = 1$ is initialized and results from the CWC and non-CWC discretizations are compared in Figure 6, in which the discretization used in case III in Section 5.1

Copyright © 2009 John Wiley & Sons, Ltd.

DOI: 10.1002/fld

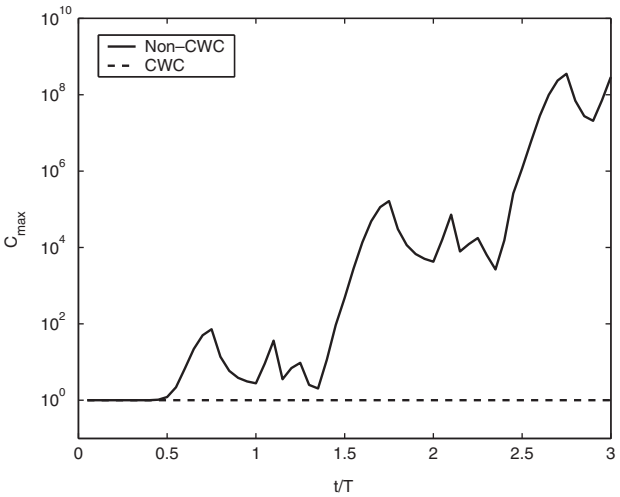


Figure 7. Time history of the maximum concentration within the domain from $t = 0$ to $3T$ in the simulation of flow with a constant concentration field ($C = 1$) over an oscillatory bottom boundary for the CWC case (dashed line) and the non-CWC case (solid line).

is employed as the non-CWC case. As shown in Figure 6, the difference between these two cases is obvious, particularly when the grid deformation is large. In the non-CWC case, the error induced by non-consistency is evident, and the concentration field is not uniform as soon as the simulation starts. The most significant errors are found at the bottom boundary where cells undergo the largest deformation. The magnitude of the error grows with time and, as a result, the simulation becomes unstable and the concentration field grows unbounded, as shown in Figure 7. In contrast, the consistent case (the left column in Figure 6 and the dashed line in Figure 7) shows a uniform concentration field throughout the simulation despite strong changes in the grid geometry.

## 6. CONCLUSION

In this paper we derived the conservation laws for flow, scalar, and momentum with the general mathematical formulation of transforming from a fixed Cartesian coordinate system to a generalized moving curvilinear coordinate system. On these types of grids, when flow calculations are carried out, the continuity equation in physical space for incompressible flow is composed of two parts, namely the instantaneous continuity equation, which is identical to that on a fixed grid and the equation governing conservation of cell geometry, which is referred to as the GCL. By employing the cell geometric operator at half time steps, we present a method in which the GCL can always be satisfied in a discrete sense under arbitrary multi-dimensional grid movement. Using this formulation for the discrete GCL then requires that the same formulation be used when discretizing the transport equations for momentum and scalars if consistency with continuity (CWC) is to be satisfied. The methods developed in this paper guarantee CWC, which can be shown to be identically satisfied if substitution of a constant scalar field into the discretized transport equations yields the same discretization for the continuity equation and the GCL.

Copyright © 2009 John Wiley & Sons, Ltd.

DOI: 10.1002/fld

Although we demonstrated that CWC can be satisfied only if the discretization schemes for scalar transport and the GCL are consistent, satisfying CWC does not guarantee the desired time accuracy since it can be limited by the time accuracy of the grid velocity. That is, application of the first-order in time approximation for the grid velocity to both scalar transport and the GCL ensures CWC, but the resulting time accuracy becomes first-order regardless of the time accuracy employed for scalar transport and the GCL. Therefore, in order to maintain time accuracy upon satisfying CWC, the grid velocity must be approximated with a time accuracy that is at least as high as that which is used for scalar transport and the GCL. We demonstrated this by developing a second-order accurate grid velocity using AB2 that ensured second-order time accuracy for the consistent AB2 formulations for scalar transport and the GCL.

The importance of satisfying the CWC condition is demonstrated with two numerical examples using a three-dimensional Navier–Stokes simulator with a generalized moving curvilinear coordinate grid. The first test case demonstrates the effects of not satisfying CWC under the influence of scalar transport due to grid motion alone and no fluid velocity. Three methods are employed, namely first that is CWC and first-order accurate in time, second that is CWC and is second-order accurate in time, and a third that is second-order accurate in time for scalar transport and first-order accurate in time for the grid and does not satisfy CWC. The results show that higher-order temporal accuracy can be achieved by means of the present discretization method for the grid velocities, and that the non-CWC method induces significant errors due to the excessive mass creation induced by the non-conservative property of the moving grid. In the second numerical example, flow is induced only due to an oscillating boundary, and this example is designed to demonstrate the effects of not satisfying CWC when the grid moves and there is fluid motion induced by motion of the boundaries. The results indicate significant errors in the scalar concentration field, particularly near the bottom where the cells are highly skewed. While the CWC method maintains a uniform concentration field in this test case, the uniform concentration field in the non-CWC case develops near-bed concentrations that grow exponentially in time.

## APPENDIX A

The cell volume obtained by Equation (17)

$$J^{-1}|_{i,j}^{n}(t) \approx \begin{vmatrix} \dfrac{\delta_\xi x_{i,j+1/2}(t)+\delta_\xi x_{i,j-1/2}(t)}{2} & \dfrac{\delta_\eta x_{i+1/2,j}(t)+\delta_\eta x_{i-1/2,j}(t)}{2} \\ \dfrac{\delta_\xi y_{i,j+1/2}(t)+\delta_\xi y_{i,j-1/2}(t)}{2} & \dfrac{\delta_\eta y_{i+1/2,j}(t)+\delta_\eta y_{i-1/2,j}(t)}{2} \end{vmatrix}$$

is approximated with a parallelogram, as shown in Figure A1, in which the centered second-order approximation is used to represent the length of its edges, e.g.

$$\delta_\xi x_{i,j}(t) = \frac{\delta_\xi x_{i,j+1/2}(t)+\delta_\xi x_{i,j-1/2}(t)}{2} + \mathcal{O}(\Delta y^2) \tag{A1}$$

Copyright © 2009 John Wiley & Sons, Ltd.

DOI: 10.1002/fld

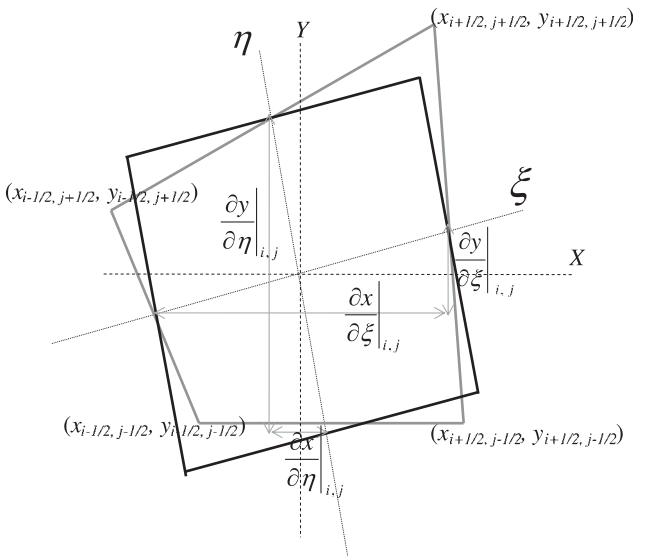


Figure A1. Depiction of a cell with an arbitrary concave shape by gray thick solid lines along with its parallelogram approximation by thick black solid lines. This shows the cell volume (area) is approximated by a parallelogram with its edges calculated by central averaging. This second-order approximation is applied to both the initial cell volume and the volume change in this study.

In the moving grid, with the definition $\delta_\xi() = ()_{i+1/2} - ()_{i-1/2}$ and $\delta_\eta() = ()_{j+1/2} - ()_{j-1/2}$, the time rate of change of the cell volume $\mathrm{d}J^{-1}|_{i,j}^{n}(t)/\mathrm{d}t$ can then be written as

$$\begin{aligned}
\frac{\mathrm{d}J^{-1}|_{i,j}^{n}(t)}{\mathrm{d}t} \approx & \begin{vmatrix} u_{g,i+1/2,j}(t) - u_{g,i-1/2,j}(t) & u_{g,i,j+1/2}(t) - u_{g,i,j-1/2}(t) \\ \dfrac{\delta_\xi y_{i,j+1/2}(t) + \delta_\xi y_{i,j-1/2}(t)}{2} & \dfrac{\delta_\eta y_{i+1/2,j}(t) + \delta_\eta y_{i-1/2,j}(t)}{2} \end{vmatrix} \\
& + \begin{vmatrix} \dfrac{\delta_\xi x_{i,j+1/2}(t) + \delta_\xi x_{i,j-1/2}(t)}{2} & \dfrac{\delta_\eta x_{i+1/2,j}(t) + \delta_\eta x_{i-1/2,j}(t)}{2} \\ v_{g,i+1/2,j}(t) - v_{g,i-1/2,j}(t) & v_{g,i,j+1/2}(t) - v_{g,i,j-1/2}(t) \end{vmatrix} \\
\approx & \left.\frac{\partial y(t)}{\partial \eta}\right|_{i,j} (u_{g,i+1/2,j}(t) - u_{g,i-1/2,j}(t)) - \left.\frac{\partial x(t)}{\partial \eta}\right|_{i,j} (v_{g,i+1/2,j}(t) - v_{g,i-1/2,j}(t)) \\
& - \left.\frac{\partial y(t)}{\partial \xi}\right|_{i,j} (u_{g,i,j+1/2}(t) - u_{g,i,j-1/2}(t)) \\
& + \left.\frac{\partial x(t)}{\partial \xi}\right|_{i,j} (v_{g,i,j+1/2}(t) - v_{g,i,j-1/2}(t))
\end{aligned} \tag{A2}$$

Copyright © 2009 John Wiley & Sons, Ltd.

DOI: 10.1002/fld

Now, recalling the volume change formulation in the present study, Equations (30)–(32), the time rate of change of the cell volume can be written in the finite-volume form as

$$\begin{aligned}\frac{\mathrm{d}J^{-1}|^n_{i,j}(t)}{\mathrm{d}t} &\approx U_{g,i+1/2,j}-U_{g,i-1/2,j}+V_{g,i,j+1/2}-V_{g,i,j-1/2}\\ &=\left(\left.\frac{\partial y(t)}{\partial\eta}\right|_{i+1/2,j}u_{g,i+1/2,j}(t)-\left.\frac{\partial y(t)}{\partial\eta}\right|_{i-1/2,j}u_{g,i-1/2,j}(t)\right)\\ &\quad-\left(\left.\frac{\partial x(t)}{\partial\eta}\right|_{i+1/2,j}v_{g,i+1/2,j}(t)-\left.\frac{\partial x(t)}{\partial\eta}\right|_{i-1/2,j}v_{g,i-1/2,j}(t)\right)\\ &\quad-\left(\left.\frac{\partial y(t)}{\partial\xi}\right|_{i,j+1/2}u_{g,i,j+1/2}(t)-\left.\frac{\partial y(t)}{\partial\xi}\right|_{i,j-1/2}u_{g,i,j-1/2}(t)\right)\\ &\quad+\left(\left.\frac{\partial x(t)}{\partial\xi}\right|_{i,j+1/2}v_{g,i,j+1/2}(t)-\left.\frac{\partial x(t)}{\partial\xi}\right|_{i,j-1/2}v_{g,i,j-1/2}(t)\right)\end{aligned}\tag{A3}$$

The difference between Equations (A2) and (A3) arises from the flux face that is used. Equation (A2) uses the approximated face at the central point $(i, j)$ while Equation (A3) uses the real face $(i\pm1/2, j\pm1/2)$. Therefore, Equation (A2) can be employed if the flow and scalar field are solved with the finite-difference formulation, while Equation (A3) must be used in the finite-volume formulation.

## APPENDIX B

Using a coordinate transformation from the Cartesian coordinate system $(x, y, z)$ to the generalized curvilinear coordinate system $(\xi, \eta, \zeta)$, the three-dimensional analogue of Equation (18) to update the cell volume, $J^{-1}|_{i,j,k}$, is given by

$$\begin{aligned}J^{-1}|^{n+1}_{i,j,k} &= J^{-1}|^n_{i,j,k}+\int_{t^n}^{t^{n+1}}(U_{g,i+1/2,j,k}(\tau)-U_{g,i-1/2,j,k}(\tau))\\ &\quad+(V_{g,i,j+1/2,k}(\tau)-V_{g,i,j-1/2,k}(\tau))+(W_{g,i,j,k+1/2}(\tau)-W_{g,i,j,k-1/2}(\tau))\,\mathrm{d}\tau\\ &= J^{-1}|^n_{i,j}+(\widetilde{U}_{g,i+1/2,j,k}-\widetilde{U}_{g,i-1/2,j,k})\Delta t+(\widetilde{V}_{g,i,j+1/2,k}-\widetilde{V}_{g,i,j-1/2,k})\Delta t\\ &\quad+(\widetilde{W}_{g,i,j,k+1/2}-\widetilde{W}_{g,i,j,k-1/2})\Delta t\end{aligned}\tag{B1}$$

where $W_g$ is the contravariant grid volume flux in the $\zeta$-direction. Again, if a constant grid velocity between $t^n$ and $t^{n+1}$ is assumed, using the intermediate metric quantities (e.g. $\partial y/\partial\eta$), the

Copyright © 2009 John Wiley & Sons, Ltd.

DOI: 10.1002/fld

three-dimensional analogues of Equations (30)–(32) are given by

$$J^{-1}|_{i,j,k}^{n+1} = J^{-1}|_{i,j,k}^{n} + \Delta t\,(U_{g,i+1/2,j,k}^{n+1/2,n} - U_{g,i-1/2,j,k}^{n+1/2,n}) + \Delta t\,(V_{g,i,j+1/2,k}^{n+1/2,n} - V_{g,i,j-1/2,k}^{n+1/2,n})$$

$$+\Delta t\,(W_{g,i,j,k+1/2}^{n+1/2,n} - V_{g,i,j,k-1/2}^{n+1/2,n}) \tag{B2}$$

where

$$U_{g,i\pm1/2,j,k}^{n+1/2,n} = \left|\begin{matrix} \dfrac{\partial y}{\partial \eta} & \dfrac{\partial y}{\partial \zeta} \\ \dfrac{\partial z}{\partial \eta} & \dfrac{\partial z}{\partial \zeta} \end{matrix}\right|_{i\pm1/2,j,k}^{n+1/2} u_{g,i\pm1/2,j,k}^{n} + \left|\begin{matrix} \dfrac{\partial z}{\partial \eta} & \dfrac{\partial z}{\partial \zeta} \\ \dfrac{\partial x}{\partial \eta} & \dfrac{\partial x}{\partial \zeta} \end{matrix}\right|_{i\pm1/2,j,k}^{n+1/2} v_{g,i\pm1/2,j,k}^{n}$$

$$+\left|\begin{matrix} \dfrac{\partial x}{\partial \eta} & \dfrac{\partial x}{\partial \zeta} \\ \dfrac{\partial y}{\partial \eta} & \dfrac{\partial y}{\partial \zeta} \end{matrix}\right|_{i\pm1/2,j,k}^{n+1/2} w_{g,i\pm1/2,j,k}^{n} \tag{B3}$$

$$V_{g,i,j\pm1/2,k}^{n+1/2,n} = \left|\begin{matrix} \dfrac{\partial y}{\partial \zeta} & \dfrac{\partial y}{\partial \xi} \\ \dfrac{\partial z}{\partial \zeta} & \dfrac{\partial z}{\partial \xi} \end{matrix}\right|_{i,j\pm1/2,k}^{n+1/2} u_{g,i,j\pm1/2,k}^{n} + \left|\begin{matrix} \dfrac{\partial z}{\partial \zeta} & \dfrac{\partial z}{\partial \xi} \\ \dfrac{\partial x}{\partial \zeta} & \dfrac{\partial x}{\partial \xi} \end{matrix}\right|_{i,j\pm1/2,k}^{n+1/2} v_{g,i,j^n\pm1/2,k}^{n}$$

$$+\left|\begin{matrix} \dfrac{\partial x}{\partial \zeta} & \dfrac{\partial x}{\partial \xi} \\ \dfrac{\partial y}{\partial \zeta} & \dfrac{\partial y}{\partial \xi} \end{matrix}\right|_{i,j\pm1/2,k}^{n+1/2} w_{g,i,j\pm1/2,k}^{n} \tag{B4}$$

and

$$W_{g,i,j,k\pm1/2}^{n+1/2,n} = \left|\begin{matrix} \dfrac{\partial y}{\partial \xi} & \dfrac{\partial y}{\partial \eta} \\ \dfrac{\partial z}{\partial \xi} & \dfrac{\partial z}{\partial \eta} \end{matrix}\right|_{i,j,k\pm1/2}^{n+1/2} u_{g,i,j,k\pm1/2}^{n} + \left|\begin{matrix} \dfrac{\partial z}{\partial \xi} & \dfrac{\partial z}{\partial \eta} \\ \dfrac{\partial x}{\partial \xi} & \dfrac{\partial x}{\partial \eta} \end{matrix}\right|_{i,j,k\pm1/2}^{n+1/2} v_{g,i,j,k\pm1/2}^{n}$$

$$+\left|\begin{matrix} \dfrac{\partial x}{\partial \xi} & \dfrac{\partial x}{\partial \eta} \\ \dfrac{\partial y}{\partial \xi} & \dfrac{\partial y}{\partial \eta} \end{matrix}\right|_{i,j,k\pm1/2}^{n+1/2} w_{g,i,j,k\pm1/2}^{n} \tag{B5}$$

Copyright © 2009 John Wiley & Sons, Ltd.

DOI: 10.1002/fld

where $u_g, v_g$, and $w_g$ are grid velocities in the $x$-, $y$-, and $z$-directions, respectively, $U_g, V_g$, and $W_g$ are the contravariant volume fluxes in the $\xi$-, $\eta$-, and $\zeta$-directions, respectively, and each determinant represents the intermediate surface component at $t = t^{n+1/2}$ normal to its associated grid velocity.

## ACKNOWLEDGEMENTS

We gratefully acknowledge the support of the ONR Coastal Geosciences Program under Grant N00014-05-1-0177 (Scientific officers: Dr Tom Drake and Dr Nathaniel Plant). Simulations were carried out on the MJM machine at the Army Research Lab Major Shared Resource Center.

## REFERENCES

1. Jin C, Xu K. A unified moving grid gas-kinetic method in Eulerian space for viscous flow computation. *Journal of Computational Physics* 2007; **222**:155–175.
2. LeVeque R. High resolution conservative algorithms for advection in incompressible flow. *SIAM Journal on Numerical Analysis* 1996; **33**:627–665.
3. Lin S, Rood RB. Multidimensional flux-form semi-Lagrangian transport schemes. *Monthly Weather Review* 1996; **119**:2046–2070.
4. Leonard BP, Lock AP, MacVean MK. Conservative explicit unrestricted-time-step multidimensional constancy-preserving advection schemes. *Monthly Weather Review* 1996; **124**:2588–2606.
5. Gross ES, Koseff JR, Monismith SG. Evaluation of advective schemes for estuarine salinity simulations. *Journal of Hydraulic Engineering* (ASCE) 1999; **45**:15–21.
6. Gross ES, Bonaventura L, Rosatti G. Consistency with continuity in conservative advection schemes for free-surface models. *International Journal for Numerical Methods in Fluids* 2002; **38**:307–327.
7. Thomas PD, Lombard CK. Geometric conservation law and its application to flow computations on moving grids. *AIAA Journal* 1979; **17**(10):1030–1037.
8. Guillard H, Farhat C. On the significance of the geometric conservation law for flow computations on moving meshes. *Computer Methods in Applied Mechanics and Engineering* 2000; **190**:1467–1482.
9. Geuzaine P, Grnadmont C, Farhat C. Design and analysis of ALE schemes with provable second-order time-accuracy for inviscid and viscous flow simulations. *Journal of Computational Physics* 2003; **191**:206–227.
10. Farhat C, Ceuzaine P, Grandmont C. The discrete geometric conservation law and the nonlinear stability of ALE schemes for the solution of flow problems on moving grids. *Journal of Computational Physics* 2001; **174**:669–694.
11. Formaggia L, Nobile F. A stability analysis for the arbitrary Lagrangian–Eulerian formulation with finite elements. *Ease–West Journal of Numerical Mathematics* 1999; **7**(2):105–131.
12. Formaggia L, Nobile F. Stability analysis of second-order time accurate schemes. *Computer Methods in Applied Mechanics and Engineering* 2004; **193**:4097–4116.
13. Thompson JF, Warsi ZUA, Mastin CW. *Numerical Grid Generation, Foundations and Applications*. Elsevier: Amsterdam, New York, 1985.
14. Hindman RG. Generalized coordinate forms of governing fluid equations and associated geometrically induced errors. *AIAA Journal* 1982; **10**:65–68.
15. Fringer OB, Armfield SW, Street RL. Reducing numerical diffusion in interfacial gravity wave simulations. *International Journal for Numerical Methods in Fluids* 2005; **49**(3):301–329.
16. Kim J, Moin P. Application of a fractional-step method to incompressible Navier–Stokes equations. *Journal of Computational Physics* 1989; **59**:308–323.
17. Zang Y, Street RL, Koseff JR. A non-staggered grid, fractional step method for time-dependent incompressible Navier–Stokes equations in curvilinear coordinates. *Journal of Computational Physics* 1994; **114**:18–33.
18. Fringer OB, Gerritsen M, Street RL. An unstructured grid, finite-volume, nonhydrostatic, parallel coastal ocean simulator. *Ocean Modelling* 2006; **14**(3–4):139–278.
19. Demirdzic I, Peric M. Space conservation law in finite volume calculation of fluid flow. *International Journal for Numerical Methods in Fluids* 1988; **8**:1037–1050.

Copyright © 2009 John Wiley & Sons, Ltd.

DOI: 10.1002/fld

20. Shyy W, Udaykumar HS, Rao MK, Smith RW. *Computational Fluid Dynamics with Moving Boundaries*. Taylor & Francis: London, 1996.
21. Hodges BR, Street RL. On simulation of turbulent nonlinear free-surface flows. *Journal of Computational Physics* 1999; **151**:425–457.
22. Stockie JM, Mackenzie JA, Russell RD. A moving mesh method for one-dimensional hyperbolic conservation laws. *SIAM Journal on Scientific Computing* 2001; **22**(5):1791–1813.
23. Cui AQ, Street RL. Large-eddy simulation of coastal upwelling flow. *Environmental Fluid Mechanics* 2004; **4**:197–223.

Copyright © 2009 John Wiley & Sons, Ltd.

DOI: 10.1002/fld